The Marriage of the FeN$_4$ Moiety and MXene Boosts Oxygen Reduction Catalysis: Fe 3d Electron Delocalization Matters

Zilan Li, Zechao Zhuang, Fan Lv, Han Zhu, Liang Zhou, Mingchuan Luo, Jiexin Zhu, Zhiquan Lang, Shihao Feng, Wei Chen,* Liqiang Mai,* and Shaojun Guo*

Iron–nitrogen–carbon (Fe–N–C) is hitherto considered as one of the most satisfactory alternatives to platinum for the oxygen reduction reaction (ORR). Major efforts currently are devoted to the identification and maximization of carbon-enclosed FeN$_4$ moieties, which act as catalytically active centers. However, fine-tuning of their intrinsic ORR activity remains a huge challenge. Herein, a twofold activity improvement of pristine Fe–N–C through introducing Ti$_3$C$_2$T$_x$ MXene as a support is realized. A series of spectroscopy and magnetic measurements reveal that the marriage of FeN$_4$ moiety and MXene can induce remarkable Fe 3d electron delocalization and spin-state transition of Fe(II) ions. The lower local electron density and higher spin state of the Fe(II) centers greatly favor the Fe d_{z^2} electron transfer, and lead to an easier oxygen adsorption and reduction on active FeN$_4$ sites, and thus an enhanced ORR activity. The optimized catalyst shows a two- and fivefold higher specific ORR activity than those of pristine catalyst and Pt/C, respectively, even exceeding most Fe–N–C catalysts ever reported. This work opens up a new pathway in the rational design of Fe–N–C catalysts, and reflects the critical influence of Fe 3d electron states in FeN$_4$ moiety supported on MXene in ORR catalysis.

The growing energy demands have kindled strong interests on the renewable energy technologies with low cost and high environmental friendliness, including fuel cells and metal–air batteries.[1] Oxygen reduction reaction (ORR) as a half reaction strictly determines the performance of these devices, but intrinsically features a sluggish kinetics.[2,3] Therefore, developing efficient cathode electrocatalysts to boost ORR is highly necessary.[3] Up to now, palladium (Pt) has been considered as the best ORR catalyst, however, its scarcity limits the large-scale commercialization.[2–4] Fortunately, various nonprecious catalysts, such as metal oxides and metal–nitrogen–carbon materials (Me–N–Cs), were widely found to have the potentials to replace Pt during this decade.[5,6]

Of these nonprecious ORR catalysts, iron–nitrogen–carbon materials (Fe–N–Cs) are one of the most promising options.[6–8] In general, their FeN$_4$ moieties serve as active sites, with typical characteristics of square-planar D$_{4h}$ local symmetry of Fe(II) ion enveloped by four-coordinated nitrogen ligands.[9] Since the Fe(II) has an uncommon intermediate spin state ($S = 1$) with an electron configuration of $d_{xy}^2 d_{yz}^2 d_{xz}^1 d_{z^2}^1$, the single d_{z^2} electron can readily penetrate the antibonding π-orbital of oxygen, rendering a high ORR activity comparable to or exceeding Pt.[9–12] To date, many efforts have been devoted into the active-site identification and geometric design for exposing more FeN$_4$ moieties.[7,12,13] However, few works emphasize the further modification of electronic structure for activity improvement, thus remaining a crucial bottleneck in catalyst development. New avenues should be opened to achieve the optimization of Fe–N–C, while supporting catalyst is considered as an effective tactic for traditional thermocatalysts.[14] It may introduce the strong interactions between Fe–N–C and substrate, and greatly alter the spin configuration of FeN$_4$ moiety. Yet, the activities and effects of supported Fe–N–C remain largely unknown.

MXenes, as a new family of 2D materials, are produced by selective etching of the A segment (such as Al) from MAX phases.[15,16] They often possess a universal formula M$_{n+1}$X$_n$T$_x$, where M is early transition metal, X denotes C and/or N, and T$_x$ represents surface terminations.[16] In light of surface hydrophilicity and electronegativity, good conductivity, and

Z. Li, Z. Zhuang, Prof. L. Zhou, J. Zhu, Z. Lang, S. Feng,
Prof. W. Chen, Prof. L. Mai
State Key Laboratory of Advanced Technology for
Materials Synthesis and Processing
International School of Materials Science and Engineering
Wuhan University of Technology
Wuhan 430070, P. R. China
E-mail: chenwei2005@whut.edu.cn; mlq518@whut.edu.cn

F. Lv, Dr. M. Luo, Prof. S. Guo
Department of Materials Science and Engineering, and BIC-ESAT
College of Engineering
Peking University
Beijing 100871, P. R. China
E-mail: guosj@pku.edu.cn

Dr. H. Zhu
School of Chemical and Material Engineering
Key Laboratory of Food Colloids and Biotechnology
Ministry of Education
Jiangnan University
Wuxi 214122, P. R. China

mechanical stability, MXenes emerge as a fascinating support, and receive widespread research interest.[17] Particularly, the electronic properties of MXenes dramatically vary with their lattice geometry and surface terminations, enabling the tunability of near-MXene surface environment and supported catalysts.[17] MXenes may therefore hold the key to unlocking the activity enhancement of Fe–N–C.

Herein, we realize a twofold enhancement for the intrinsic ORR activity of pristine iron phthalocyanine (FePc) catalyst, through introducing $Ti_3C_2T_x$ as a support for the first time. FePc, an early Fe–N–C prototype with typical FeN_4 moiety and very Pt-like ORR activity, is chosen as a model catalyst.[18] Coupling FePc with $Ti_3C_2T_x$ MXene leads to remarkable Fe 3d electron delocalization and spin configuration changes. These strong interactions make active FeN_4 sites more readily absorb reaction species involved, thus boosting ORR catalysis. Our

optimized catalyst exhibits a two- and fivefold higher specific ORR activity than those of pure FePc and Pt/C, respectively, even exceeding most Fe–N–C catalysts ever reported under the same experimental conditions. This development opens up a new avenue to rational design of efficient Fe–N–C catalysts by MXene supporting, and also provides in-depth understanding of the roles of 3d electron states in active FeN_4 moiety.

We first obtained the $FePc/Ti_3C_2T_x$ hybrid catalysts by a facile route through homogeneous dispersion and self-assembly of FePc and $Ti_3C_2T_x$ MXene in dimethylformamide (DMF) solution under ultrasonic conditions. Next, the morphology of pristine $Ti_3C_2T_x$ and FePc-coated one was disclosed by electron microscopy. The scanning electron microscopy (SEM) image shows that the pristine $Ti_3C_2T_x$ exhibits an accordion-like structure, obtained through etching bulk Ti_3AlC_2 particles (MAX) to extract Al (**Figure 1**a). For $FePc/Ti_3C_2T_x$, the $Ti_3C_2T_x$ retains its
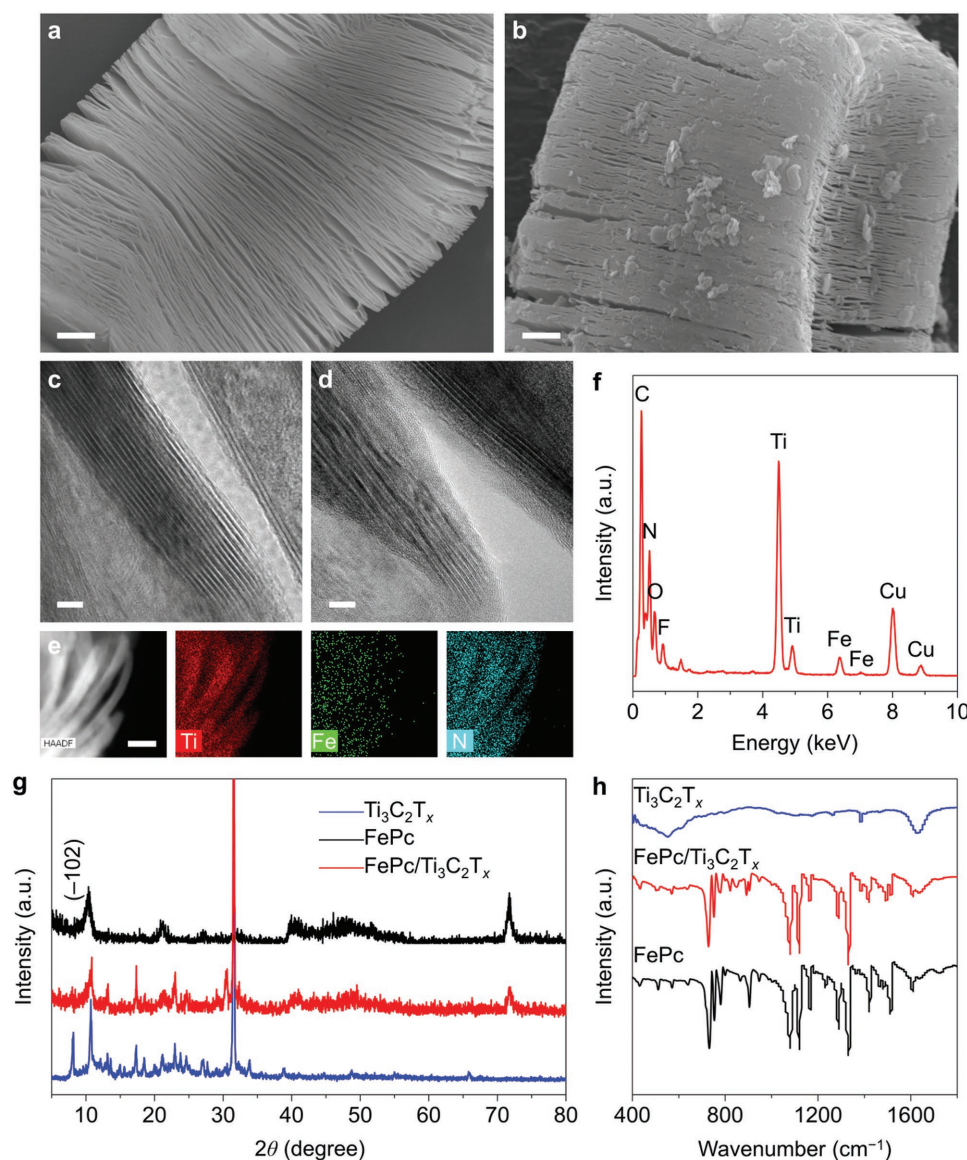
Figure 1. a,b) SEM and c,d) TEM images of pristine $Ti_3C_2T_x$ and $FePc/Ti_3C_2T_x$. The scale bars are 1 µm (a,b) and 5 nm (c,d). e) EDS mapping images and f) line-scan spectrum of $FePc/Ti_3C_2T_x$. The scale bar is 20 nm. g) XRD patterns and h) FTIR spectra of pristine $Ti_3C_2T_x$, FePc, and $FePc/Ti_3C_2T_x$.

initial layered structure, while the layer surfaces become much rougher, and the interlayer spacing also appears to be smaller (Figure 1b and Figure S1, Supporting Information). The transmission electron microscopy (TEM) images further demonstrate that FePc molecules are closely attached on $Ti_3C_2T_x$ surfaces, forming an amorphous thin coating (Figure 1c,d, and Figure S2, Supporting Information). Note that the high-energy electrons under the operation of an electron microscope can readily destroy the crystal structure of FePc molecules on MXene surface, although the X-ray diffraction (XRD) patterns indicate that the grain size of FePc does not change after supporting and it should not be an amorphous phase (Figure 1g). Brunauer–Emmett–Teller (BET) method was also employed to obtain the specific surface area and pore size distribution of Ti_3AlC_2, $Ti_3C_2T_x$, and FePc/$Ti_3C_2T_x$, respectively (Figure S3, Supporting Information). Our results indicate that $Ti_3C_2T_x$ possesses a much larger specific surface area (14.7 m^2 g^{-1}) than that of Ti_3AlC_2 (1.3 m^2 g^{-1}), while the loading of FePc molecules leads to an obvious decreased surface area of 2.2 m^2 g^{-1}, in good agreement with the SEM and TEM results. Both energy-dispersive X-ray spectroscopy (EDS) elemental mapping images and spectrum feature a uniform distribution of Ti, Fe, and N elements, and also confirm this strong combination between FePc and $Ti_3C_2T_x$ (Figure 1e,f). Moreover, the weight ratio of Fe in FePc/$Ti_3C_2T_x$ was determined to be 4.09 wt% from inductively coupled plasma mass spectrometry (ICP-MS) analysis, indicating that the mass loading of FePc is ≈41.5% (Table S1, Supporting Information). Next, the phase and surface functional groups of samples were analyzed by XRD and Fourier transform infrared (FTIR) spectroscopy. The diffraction peak located at ≈39° for (104) plane of original Ti_3AlC_2 is absent in the XRD pattern of $Ti_3C_2T_x$, suggesting the successful removal of Al layers by etching (Figure S4, Supporting Information). EDS mapping images also confirm this complete elimination (Figure S5, Supporting Information). In the pattern of FePc/$Ti_3C_2T_x$, the sharp peak located at ≈32° can be assigned to $Ti_3C_2T_x$,[16] confirming the existence of $Ti_3C_2T_x$ support (Figure 1g). The disappearance of the diffraction peak at a small ≈8° suggests that FePc molecules should entry the MXene interlayer and weaken their highly ordered arrangement. Besides, the FTIR spectrum of FePc/$Ti_3C_2T_x$ matches well with that of FePc, also suggesting the successful coating of FePc on $Ti_3C_2T_x$ (Figure 1h). Particularly, the band at 729 cm^{-1} can be attributed to C−H out-of-plane stretching vibration in FePc macrocycle, while the bands at 1608, 1075, and 1117 cm^{-1} can be assigned to C−H in-plane deformation. The band at 1331 cm^{-1} can belong to C=C or C=N stretching vibration. For neighboring functional groups of Fe center, the band at 751 cm^{-1}, corresponding to benzene deformation, isoindol deformation, and Fe−N stretching, and another one at 1413 cm^{-1}, ascribing to C−H in-plane pyrrole bending, C−N, and C−C stretching, were observed. The band at 1727 cm^{-1} can be assigned to metal axial ligand of FePc, but it vanishes after the introduction of $Ti_3C_2T_x$.[19] In addition, the band at 3430 cm^{-1}, corresponding to surface hydroxyl groups of $Ti_3C_2T_x$, was also observed in the spectrum of FePc/$Ti_3C_2T_x$ (Figure S6, Supporting Information).[20] These results are in agreement with the microscopy images, indicating the successful association between FePc and $Ti_3C_2T_x$.

To investigate the ORR activity of FePc/$Ti_3C_2T_x$, the rotating disk electrode (RDE) voltammetry tests were carried out in 0.1 M KOH electrolyte solution saturated with O_2. Before the electrochemical tests, all the catalysts were uniformly loaded onto commercial Vulcan XC-72R carbon to obtain the catalyst paste. The recorded linear sweep voltammetry (LSV) curves (**Figure 2**a) show a much more positive half-wave potential ($E_{1/2}$) of 0.86 V versus RHE for pure FePc than that of commercial Pt/C (0.84 V vs RHE), indicating that pure FePc possesses a high intrinsic ORR activity. After the introduction of $Ti_3C_2T_x$, a remarkable ORR activity enhancement of FePc was observed, where the $E_{1/2}$ of FePc/$Ti_3C_2T_x$ exhibits a more positive shift of ≈26 mV. Their ORR activities at 0.90 and 0.85 V versus RHE are further compared in Figure 2b,c. Notably, FePc/$Ti_3C_2T_x$ shows a kinetic current density (J_k) of 15.5 mA cm^{-2} at 0.90 V versus RHE, far higher than those of pure FePc and Pt/C (6.9 and 2.6 mA cm^{-2}). At both electrode potentials, our hybrid catalyst delivers a more than twofold increase in ORR activity than that of FePc, and fivefold higher activity against that of Pt/C. So far, this specific activity for ORR is one of the highest among the Fe−N−C systems and other FePcs supported on different substrates (including carbon nanotube, graphene, carbon black, and pyrolytic graphite) reported in the literatures (Tables S2 and S3, Supporting Information). We then calculated the turnover frequency (TOF) to compare the intrinsic activity of ORR catalysts (Figure 2d). The TOF of active FeN_4 sites within FePc/$Ti_3C_2T_x$ at 0.80 V versus RHE is determined to be 15.1e s^{-1} $site^{-1}$, fourfold higher than that of pure FePc (3.9e s^{-1} $site^{-1}$). The LSV voltammograms were further recorded at different rotation rates to obtain more ORR kinetics information. It is obvious that the current density of FePc/$Ti_3C_2T_x$ increases with the increase of rotation rate from 400 to 2500 rpm (Figure 2e). The corresponding Koutecky–Levich plots at various potentials exhibit good linearity, and the calculated electron transfer numbers are highly close to 4, indicating a four-electron reduction pathway (inset of Figure 2e and Figure S7, Supporting Information). This $4e^-$ reduction mechanism of FePc/$Ti_3C_2T_x$ was also confirmed by rotating ring disk electrode (RRDE) voltammetry tests (Figure 2f), showing an ultralow H_2O_2 yield (below 1%). We also investigated the ORR performance of FePc/$Ti_3C_2T_x$ catalysts with different weight ratios (Figure S8, Supporting Information). The results demonstrate that an optimal mass loading of FePc can maximize the synergetic effects and lead to the highest ORR activity. Besides, long-term stability is another prerequisite for the practicability of fuel cells and metal–air batteries. A chronoamperometric i–t test of FePc/$Ti_3C_2T_x$ displays a much smaller loss of current density compared with that of commercial Pt/C. Meanwhile, $Ti_3C_2T_x$ MXene supporting can improve the stability of FePc molecules (Figure S9, Supporting Information). The ORR current density of FePc/$Ti_3C_2T_x$ remains 74% after a continuous measurement, while 65 and 49% of the current density are retained for pure FePc and Pt/C, respectively.

Such a remarkable activity enhancement should come from the possible interactions across the FePc/$Ti_3C_2T_x$ interface. Multiple spectroscopies were thus used to glean the electronic structure changes of FeN_4 moiety before and after coupling FePc with $Ti_3C_2T_x$. The survey spectra of X-ray photoelectron spectroscopy (XPS) demonstrates the existence of

ADVANCED
SCIENCE NEWS
www.advancedsciencenews.com

ADVANCED
MATERIALS
www.advmat.de

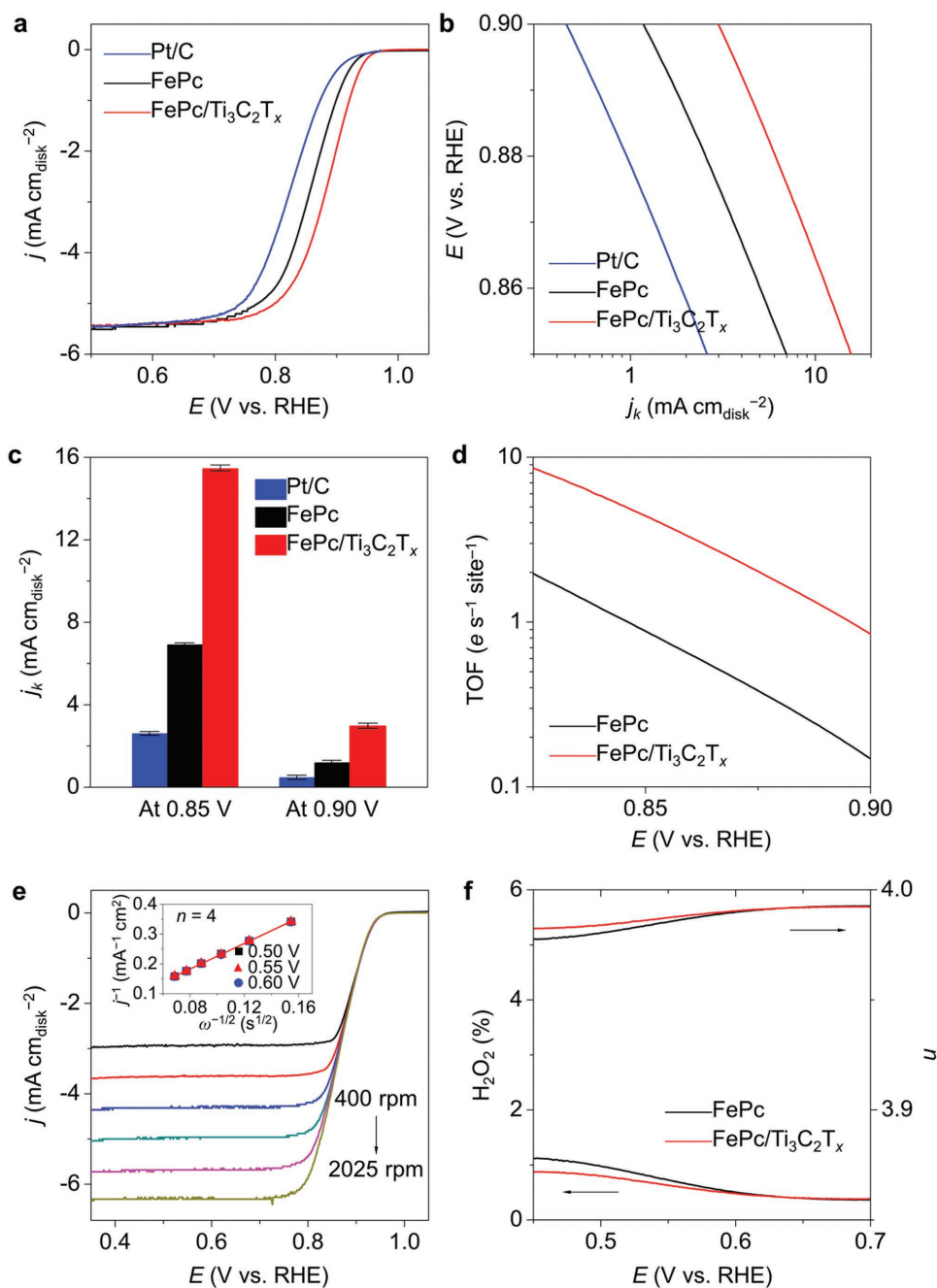**Figure 2.** a) LSV curves, b) Tafel plots, and c) kinetic current density (J_k) at 0.9 and 0.85 V versus RHE of pristine FePc, FePc/Ti$_3$C$_2$T$_x$, and Pt/C. d) Turnover frequency (TOF) of active FeN$_4$ sites in FePc and FePc/Ti$_3$C$_2$T$_x$. e) LSV curves of FePc/Ti$_3$C$_2$T$_x$ at different rotation rates of 400, 625, 900, 1225, 1600, and 2025 rpm. The inset in (e) shows the corresponding Koutecky–Levich plots at different potentials. f) Percentage of H$_2$O$_2$ released and electron transfer numbers (n) of pristine FePc and FePc/Ti$_3$C$_2$T$_x$.

Ti, Fe, N, C, O, and F (Figure S10, Supporting Information). The O and F signals may belong to the hydroxyl and fluorine terminations of Ti$_3$C$_2$T$_x$, respectively. Regarding XPS narrow scans, the Fe 2p$_{3/2}$ and Fe 2p$_{1/2}$ peaks in the spectrum of pure FePc were positioned at 710.4 and 724.5 eV, while after coupling Ti$_3$C$_2$T$_x$, both peaks were shifted to 711.9 and 725.7 eV (**Figure 3**a). Although weak XPS signals of Fe 2p exhibit a modest signal-to-noise ratio, this obvious Fe 2p peak-shift toward higher binding energy confirms the strong interactions

between Ti$_3$C$_2$T$_x$ and FeN$_4$ moiety, and the interactions greatly decrease the local electron density of Fe centers.[21,22] Next, ultraviolet photoelectron spectroscopy (UPS) was utilized to investigate the band structure of FePc/Ti$_3$C$_2$T$_x$. The cutoff energy (E_{cutoff}) of FePc and FePc/Ti$_3$C$_2$T$_x$ is 17.1 and 17.2 eV, while both the E_F are 0 eV (Figure 3b). Accordingly, their work functions (e_Φ) can be calculated to be 4.1 and 4.0 eV by the following equation, $e_\Phi = h\nu - |E_{cutoff} - E_F|$. We also obtained the valence band maximum (E_V) or highly occupied molecular
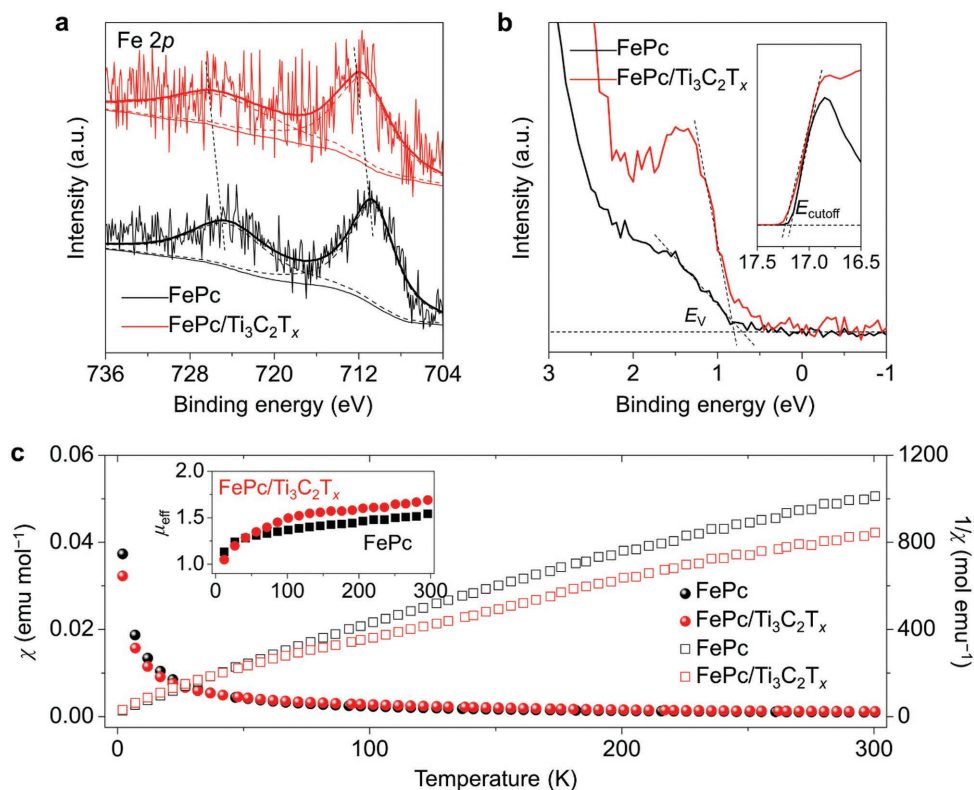
Figure 3. a) Fe 2p XPS, b) UPS spectra, and c) χ_m and $1/\chi_m$ plots of pristine FePc and FePc/Ti$_3$C$_2$T$_x$. The inset in (c) shows the comparison of μ_{eff} for pristine FePc and FePc/Ti$_3$C$_2$T$_x$.

orbital (HOMO), which is estimated to be 0.6 and 0.8 eV for FePc and FePc/Ti$_3$C$_2$T$_x$, respectively, rendering that the E_V or HOMO shifts to lower energy after the introduction of Ti$_3$C$_2$T$_x$ (inset of Figure 3b). Generally, most valence electrons of FePc concentrate on Fe(II) center, and their behavior contributes to the d states.[23] The changes of e_Φ and E_V demonstrate that the electrons within FePc framework after Ti$_3$C$_2$T$_x$ supporting are more spatially stable, and that the 3d band center of Fe(II) changes. In other words, the electron density of FeN$_4$ moiety distributes more thinly at the Fe(II) center, while more densely at the nitrogen ligands, inducing an Fe 3d electron delocalization. This finding is in decent agreement with the XPS results, and should be due to the support effects of Ti$_3$C$_2$T$_x$ MXene containing rich hydroxyl and fluorine terminations with high electronegativity, which can strongly interact with FeN$_4$ moieties and stabilize the HOMO by reducing the electron density of Fe(II). Such interactions between FePc and MXene should originate from intermolecular van der Waals forces or hydrogen bonding without obvious electron transfer. Ultraviolet–visible spectra (UV–vis) were also recorded (Figure S11, Supporting Information). Three distinct absorption peaks at ≈590, 450, and 300 nm were observed, corresponding to the Q, satellite, and Soret bands, respectively. Because FePc molecule features a D$_{4h}$ local symmetry, its electronic transitions can be characterized as follows: the Q band, which belongs to a lower energy transition, is due to a$_{1u}$ → e$_g$ from HOMO to LUMO, while the Soret band to b$_{2u}$, a$_{2u}$ → e$_g$ transitions.[22,24] After the introduction of Ti$_3$C$_2$T$_x$, both the Soret and Q bands exhibit a slight blueshift,

indicating an increase in the transition energy of HOMO → LUMO. Accordingly, we confirm that the HOMO shifts toward lower energy, and Fe 3d electrons indeed delocalize. For ORR catalysis, which involves the adsorption and desorption of oxygen species, a decreased electron density around Fe(II) centers with strong delocalization greatly optimizes the orbital overlap of Fe 3d with O$_2$ 2p, and favors the Fe d$_{z^2}$ electron jumping into O 2p orbitals, therefore boosting oxygen adsorption on FeN$_4$ moieties and the kinetics of ORR.

We also accomplished the temperature-dependent magnetic susceptibility (M–T) measurement, electron spin resonance (ESR) spectroscopy, and Mössbauer spectroscopy to unravel the electron spin configuration of FeN$_4$ moiety. Figure 3c shows a nearly temperature-independent paramagnetism for both FePc and FePc/Ti$_3$C$_2$T$_x$. From the $1/\chi_m$ plots, we can find that the introduction of Ti$_3$C$_2$T$_x$ weakens the paramagnetic state of FeN$_4$ moiety. This indicates that less free electrons with Pauli paramagnetism travel around the Fe(II) center, in good agreement with the XPS and UPS results. Besides, we further obtained the effective magnetic moment (μ_{eff}), which correlates with the number of unpaired d electron (n) of Fe(II) ion via the following equation (inset of Figure 3c)

$$2.828\sqrt{\chi_m T} = \mu_{eff} = \sqrt{n(n+2)} \qquad (1)$$

The increase of μ_{eff} demonstrates that the number of unpaired d electron of Fe(II) ions in FePc/Ti$_3$C$_2$T$_x$ is much larger than pristine FePc. This indicates that more singly
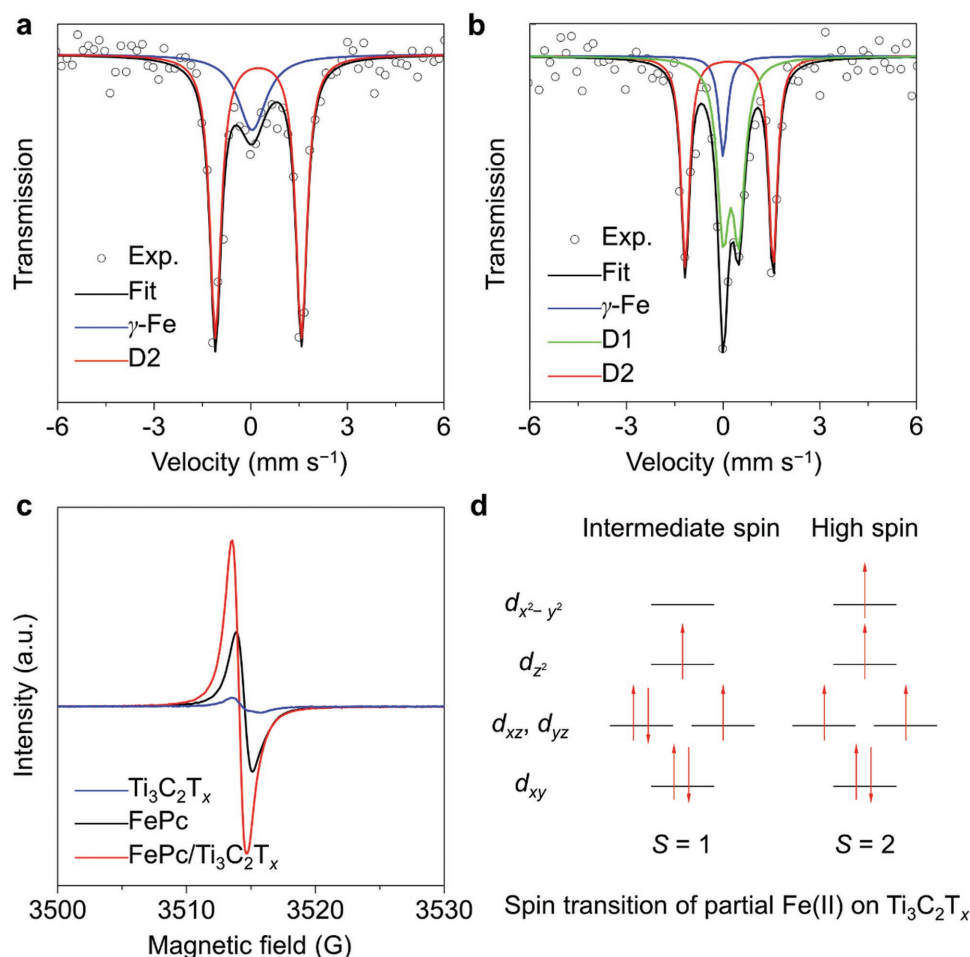
ADVANCED
SCIENCE NEWS

www.advancedsciencenews.com

ADVANCED
MATERIALS

www.advmat.de

Figure 4. a,b) ^{57}Fe Mössbauer transmission spectra and their deconvolution of pristine FePc and FePc/Ti$_3$C$_2$T$_x$. c) X-band ESR spectra of pristine Ti$_3$C$_2$T$_x$, FePc, and FePc/Ti$_3$C$_2$T$_x$. d) Schematic representation of the spin transition of partial Fe(II) on Ti$_3$C$_2$T$_x$.

occupied 3d electrons readily transfer into antibonding π-orbital of oxygen and manifest a much higher ORR activity. The ESR spectra in **Figure 4**c and Figure S12 (Supporting Information) present an obvious shift and signal reinforcement after Ti$_3$C$_2$T$_x$ supporting. As is well known, an unpaired electron that gains or loses angular momentum can alter the value of its *g* factor, and interactions of an unpaired electron with its environment also affect the shape of ESR spectra. Thus, our results indicate the changes in both 3d electron-spin configuration and chemical environment of Fe(II) centers. More detailed information can be obtained via Mössbauer spectroscopy (Figure 4a,b). The ^{57}Fe Mössbauer spectrum of pristine FePc was fitted with a D$_2$ doublet and a singlet, where the former can be assigned to intermediate-spin Fe(II) in the square-planar FeN$_4$ moiety, and the latter near zero velocity can be allocated to γ-Fe. As for Ti$_3$C$_2$T$_x$ supported FePc, the spectrum shows an unequivocally additional D$_1$ doublet belonging to high-spin Fe(II) with an electron configuration of d$_{xy}$²d$_{yz}$¹d$_{xz}$¹d$_{z^2}$¹d$_{x^2-y^2}$¹, in decent agreement with the *M−T* results, which reveal more unpaired electrons generated after coupling Ti$_3$C$_2$T$_x$ (Figure 4d).[11,25] In addition, a decreased isomer shift (δ) of the spectrum of FePc/Ti$_3$C$_2$T$_x$ compared to that of pure FePc (Table S4, Supporting Information) demonstrates an increase in the density

of s electron around Fe(II) centers. This shift that originates from a weakened shielding effect of Fe 3d electrons can also reveal an Fe 3d electron delocalization.[26] Therefore, we can conclude that the strong interactions between FeN$_4$ moieties and Ti$_3$C$_2$T$_x$ MXene greatly induce the electron density redistribution and spin-state transition through van der Waals forces or hydrogen bonding. In principle, intermediate- and high-spin Fe(II) possess different electronic configurations of d$_{xy}$²d$_{yz}$²d$_{xz}$¹d$_{z^2}$¹ and d$_{xy}$²d$_{yz}$¹d$_{xz}$¹d$_{z^2}$¹d$_{x^2-y^2}$¹, respectively. Although they both, possessing a singly filled d$_{z^2}$ orbital, are capable to induce the end-on O$_2$ adsorption and subsequent reduction on FeN$_4$ moiety, a high-spin Fe(II) center (*S* = 2) should perform much higher electrophilicity. In fact, an optimal electrophilicity of active FeN$_4$ sites leads to a neither too weak nor too strong bond strength between the oxygen species and catalyst surface, and induces a higher intrinsic ORR activity.[27]

In summary, we realize a twofold intrinsic activity improvement of pristine Fe−N−C catalyst for the first time by selecting FePc and Ti$_3$C$_2$T$_x$ MXene as model catalyst and support, respectively. Since Ti$_3$C$_2$T$_x$ MXene possesses rich surface terminations, including hydroxyl and fluorine, they can strongly interact with four-coordinated Fe(II) and weaken Fe−N bonding when FeN$_4$ moiety adheres to Ti$_3$C$_2$T$_x$ surface through van der Waals forces

or hydrogen bonding. Our XPS, UPS, UV–vis, ESR, Mössbauer spectroscopy, and magnetic susceptibility results reveal these interaction indeed lead to remarkable Fe 3d electron delocalization and spin-state transition of Fe(II) ions. Particularly, the local electron density of FeN_4 moiety greatly redistributes, and more unpaired d electrons are generated through a change in electron configuration from $d_{xy}^2 d_{yz}^2 d_{xz}^1 d_{z^2}^1$ to $d_{xy}^2 d_{yz}^1 d_{xz}^1 d_{z^2}^1 d_{x^2-y^2}^1$, yielding an easier dioxygen adsorption and reduction, and thus enhanced ORR activity. This $FePc/Ti_3C_2T_x$ catalyst demonstrates a two- and fivefold higher specific ORR activity than those of pristine FePc and Pt/C, respectively, even exceeding most Fe—N—C catalysts ever reported. Our findings open up a new avenue to design highly efficient Fe—N—C catalysts by MXene supporting and related electronic effects, and emphasize the critical roles of Fe 3d electron states in FeN_4 moiety toward ORR catalysis.

Supporting Information

Supporting Information is available from the Wiley Online Library or from the author.

Conflict of Interest

The authors declare no conflict of interest.

[1] a) M. Asadi, B. Sayahpour, P. Abbasi, A. T. Ngo, K. Karis, J. R. Jokisaari, C. Liu, B. Narayanan, M. Gerard, P. Yasaei, *Nature* **2018**, *555*, 502; b) C. C. Duan, J. H. Tong, M. Shang, S. Nikodemski, M. Sanders, S. Ricote, A. Almansoori, R. O'Hayre, *Science* **2015**, *349*, 1321; c) A. Dutta, R. A. Wong, W. Park, K. Yamanaka, T. Ohta, Y. Jung, H. R. Byon, *Nat. Commun.* **2018**, *9*, 680.

[2] a) Y. Nie, Bing, H. S. Liu, L. Zhang, D. Ghosh, J. J. Zhang, *Chem. Soc. Rev.* **2010**, *39*, 2184; b) Y. Nie, L. Li, Z. D. Wei, *Chem. Soc. Rev.* **2015**, *44*, 2168.

[3] a) J. J. Greeley, I. E. L. Stephens, A. S. Bondarenko, T. P. Johansson, H. A. Hansen, T. F. Jaramillo, J. Rossmeisl, I. Chorkendorff, J. K. Norskov, *Nat. Chem.* **2009**, *1*, 552; b) X. Q. Huang, Z. P. Zhao, L. Cao, Y. Chen, E. B. Zhu, Z. Y. Lin, M. F. Li, A. M. Yan, A. Zettl, Y. M. Wang, X. F. Duan, T. Mueller, Y. Huang, *Science* **2015**, *348*, 1230.

[4] a) X. Wang, S. I. Choi, L. T. Roling, M. Luo, C. Ma, L. Zhang, M. F. Chi, J. Y. Liu, Z. X. Xie, J. A. Herron, M. Mavrikakis, Y. N. Xia, *Nat. Commun.* **2015**, *6*, 7594; b) C. Z. Zhu, H. Li, S. F. Fu, D. Du, Y. H. Lin, *Chem. Soc. Rev.* **2016**, *45*, 517.

[5] a) S. Gadipelli, T. T. Zhao, S. A. Shevlin, Z. X. Guo, *Energy Environ. Sci.* **2016**, *9*, 1661; b) W. T. Hong, M. Risch, K. A. Stoerzinger, A. Grimaud, J. Suntivich, Y. Shao-Horn, *Energy Environ. Sci.* **2015**, *8*, 1404; c) H. W. Liang, W. Wei, Z. S. Wu, X. L. Feng, K. Mullen, *J. Am. Chem. Soc.* **2013**, *135*, 16002; d) H. W. Liang, X. D. Zhuang, S. Bruller, X. L. Feng, K. Mullen, *Nat. Commun.* **2014**, *5*, 4973; e) Y. Y. Liang, Y. G. Li, H. L. Wang, J. G. Zhou, J. Wang, T. Regier, H. J. Dai, *Nat. Mater.* **2011**, *10*, 780; f) G. Wu, K. L. More, C. M. Johnston, P. Zelenay, *Science* **2011**, *332*, 443; g) J. T. Zhang, Z. H. Zhao, Z. H. Xia, L. M. Dai, *Nat. Nanotechnol.* **2015**, *10*, 444; h) A. Zitolo, N. Ranjbar-Sahraie, T. Mineva, J. K. Li, Q. Y. Jia, S. Stamatin, G. F. Harrington, S. M. Lyth, P. Krtil, S. Mukerjee, E. Fonda, F. Jaouen, *Nat. Commun.* **2017**, *8*, 957; i) J. H. Zagal, F. Bedioui, *Electrochemistry of N₄ Macrocyclic Metal Complexes*, Springer, Berlin **2016**, pp. 1–170.

[6] Q. Wang, Z. Y. Zhou, Y. J. Lai, Y. You, J. G. Liu, X. L. Wu, E. Terefe, C. Chen, L. Song, M. Rauf, N. Tian, S. G. Sun, *J. Am. Chem. Soc.* **2014**, *136*, 10882.

[7] P. Z. Chen, T. P. Zhou, L. L. Xing, K. Xu, Y. Tong, H. Xie, L. D. Zhang, W. S. Yan, W. S. Chu, C. Z. Wu, Y. Xie, *Angew. Chem., Int. Ed.* **2017**, *56*, 610.

[8] a) Y. J. Chen, S. F. Ji, Y. G. Wang, J. C. Dong, W. X. Chen, Z. Li, R. A. Shen, L. R. Zheng, Z. B. Zhuang, D. S. Wang, Y. D. Li, *Angew. Chem., Int. Ed.* **2017**, *56*, 6937; b) H. J. Shen, E. Gracia-Espino, J. Y. Ma, K. T. Zang, J. Luo, L. Wang, S. S. Gao, X. Mamat, G. Z. Hu, T. Wagberg, S. J. Guo, *Angew. Chem., Int. Ed.* **2017**, *56*, 13800; c) R. Jasinski, *Nature* **1964**, *201*, 1212.

[9] N. Ramaswamy, U. Tylus, Q. Jia, S. Mukerjee, *J. Am. Chem. Soc.* **2013**, *135*, 15443.

[10] U. I. Kramm, N. Larouche, D. Schmeisser, J. P. Dodelet, *J. Am. Chem. Soc.* **2014**, *136*, 978.

[11] J. Li, G. Shraboni, W. Liang, M. T. Sougrati, F. Jaouen, H. Barr, M. K. Samuel, M. C. Geoff, C. Ma, X. Yuan, *Energy Environ. Sci.* **2016**, *9*, 2418.

[12] A. Zitolo, V. Goellner, V. Armel, M. T. Sougrati, T. Mineva, L. Stievano, E. Fonda, F. Jaouen, *Nat. Mater.* **2015**, *14*, 937.

[13] a) Q. Jia, N. Ramaswamy, H. Hafiz, U. Tylus, K. Strickland, G. Wu, B. Barbiellini, A. Bansil, E. F. Holby, P. Zelenay, *ACS Nano* **2015**, *9*, 12496; b) D. Malko, A. Kucernak, T. Lopes, *Nat. Commun.* **2016**, *7*, 13285; c) E. Proietti, F. Jaouen, M. Lefèvre, N. Larouche, J. Tian, J. Herranz, J.-P. Dodelet, *Nat. Commun.* **2011**, *2*, 416; d) M. L. Xiao, J. B. Zhu, L. G. Feng, C. P. Liu, W. Xing, *Adv. Mater.* **2015**, *27*, 2521.

[14] a) G. Prieto, J. Zecevic, H. Friedrich, K. P. de Jong, P. E. de Jongh, *Nat. Mater.* **2013**, *12*, 34; b) G. N. Vayssilov, Y. Lykhach, A. Migani, T. Staudt, G. P. Petrova, N. Tsud, T. Skala, A. Bruix, F. Illas, K. C. Prince, V. Matolin, K. M. Neyman, J. Libuda, *Nat. Mater.* **2011**, *10*, 310.

[15] a) B. Anasori, M. R. Lukatskaya, Y. Gogotsi, *Nat. Rev. Mater.* **2017**, *2*, 16098; b) F. Shahzad, M. Alhabeb, C. B. Hatter, B. Anasori, H. S. Man, C. M. Koo, Y. Gogotsi, *Science* **2016**, *353*, 1137; c) N. K. Chaudhari, H. Jin, B. Kim, S. B. Du, H. J. Sang, K. Lee, *J. Mater. Chem. A* **2017**, *5*, 24564.

[16] M. Naguib, M. Kurtoglu, V. Presser, J. Lu, J. Niu, M. Heon, L. Hultman, Y. Gogotsi, M. W. Barsoum, *Adv. Mater.* **2011**, *23*, 4248.

[17] a) S. T. Hunt, M. Milina, A. C. Alba-Rubio, C. H. Hendon, J. A. Dumesic, Y. Román-Leshkov, *Science* **2016**, *352*, 974; b) T. Y. Ma, J. L. Cao, M. Jaroniec, S. Z. Qiao, *Angew. Chem., Int. Ed.* **2016**, *55*, 1138; c) M. Naguib, O. Mashtalir, J. Carle, V. Presser, J. Lu, L. Hultman, Y. Gogotsi, M. W. Barsoum, *ACS Nano* **2012**, *6*, 1322; d) J. Ran, G. Gao, F. T. Li, T. Y. Ma, A. Du, S. Z. Qiao, *Nat. Commun.* **2017**, *8*, 13907; e) L. Zhao, B. Dong, S. Li, L. Zhou, L. Lai, Z. Wang, S. Zhao, M. Han, K. Gao, M. Lu, *ACS Nano* **2017**, *11*, 5800.

[18] a) R. Baker, D. P. Wilkinson, J. Zhang, *Electrochim. Acta* **2008**, *53*, 6906; b) G. Dong, M. Huang, L. Guan, *Phys. Chem. Chem. Phys.* **2012**, *14*, 2557; c) S. Zhang, H. Zhang, X. Hua, S. Chen, *J. Mater. Chem. A* **2015**, *3*, 10013; d) S. Gupta, D. Tryk, I. Bae, W. Aldred, E. Yeager, *J. Appl. Electrochem.* **1989**, *19*, 19.

[19] a) R. Aroca, A. Thedchanamoorthy, *Chem. Mater.* **1995**, *7*, 69; b) W. Gao, L. B. Alemany, L. Ci, P. M. Ajayan, *Nat. Chem.* **2009**, *1*, 403.

[20] M. Acik, C. Mattevi, C. Gong, G. Lee, K. Cho, M. Chhowalla, Y. J. Chabal, *ACS Nano* **2010**, *4*, 5861.

[21] R. Cao, R. Thapa, H. Kim, X. Xu, K. M. Gyu, Q. Li, N. Park, M. Liu, J. Cho, *Nat. Commun.* **2014**, *4*, 2076.

[22] Y. Jiang, Y. Lu, X. Lv, D. Han, Q. Zhang, L. Niu, W. Chen, *ACS Catal.* **2013**, *3*, 1263.

[23] a) I. M. Billas, A. Châtelain, W. A. de Heer, *Science* **1994**, *265*, 1682; b) E. K. Li, K. H. Johnson, D. E. Eastman, J. L. Freeouf, *Phys. Rev. Lett.* **1974**, *32*, 470.

[24] a) S. Mathew, A. Yella, P. Gao, R. Humphrybaker, B. F. Curchod, N. Ashariastani, I. Tavernelli, U. Rothlisberger, M. K. Nazeeruddin, M. Grätzel, *Nat. Chem.* **2014**, *6*, 242; b) G. Yang, Y. L. Wang, J. J. Xu, H. W. Lei, C. Chen, H. Q. Shan, X. Y. Liu, Z. X. Xu, G. J. Fang, *Nano Energy* **2017**, *31*, 322.

[25] R. Sielemann, Y. Kobayashi, Y. Yoshida, H. P. Gunnlaugsson, G. Weyer, *Phys. Rev. Lett.* **2008**, *101*, 137206.

[26] C. A. Melendres, *J. Phys. Chem.* **1980**, *84*, 1936.

[27] a) K. Ray, F. Heims, M. Schwalbe, W. Nam, *Curr. Opin. Chem. Biol.* **2015**, *25*, 159; b) H. Yu, L. Shang, T. Bian, R. Shi, G. I. Waterhouse, Y. Zhao, C. Zhou, L. Z. Wu, C. H. Tung, T. Zhang, *Adv. Mater.* **2016**, *28*, 5080.